Characterization of Low-velocity Impact Fracture Behaviour of Rigid Foam by Single Edge Notched Bend Specimens

Victor Rizov

Department of Technical Mechanics, University of Architectura, Civil Enginering and Geodesy
1 Chr. Smirnensky blvd., 1046 – Sofia, Bulgaria

V_RIZOV_FHE@UACG.BG

Abstract

Impact mixed-mode I/II fracture experiments were carried-out on rigid foam using single edge notched bend (SENB) specimens with inclined notch. A drop-weight rig was used to perform the low-velocity impact fracture tests. SENB specimens with different notch inclination were tested at various impact potential energies by varying the drop-height in order to determine the critical impact potential energy at which the crack growth is initiated from the notch tip. Three-dimensional linear-elastic finite element simulations of impact behavior of the SENB specimens were carried-out. The virtual crack closure technique was applied to analyze the strain energy release rate under impact loading. The impact fracture toughness was characterized in terms of the critical dynamic strain energy release rate at the onset of crack growth. It was found that the critical dynamic strain energy release rate decreases with increase of notch inclination. This finding was attributed to the decrease of the mode II component of the loading. SENB specimens with different notch inclination were tested also under static loading. The static fracture toughness was extracted from the test data by the virtual crack closure technique in conjunction with finite element simulations. It was found that the impact fracture toughness of the rigid foam investigated is between 22.4 % and 32 % lower than the static one at various notch inclinations. This finding indicates that the static fracture toughness should not be used in the fracture mechanics based design of rigid foam structures which are subjected to impact loading during their lifetime.

Keywords

Low-velocity Impact; Fracture Behavior; Rigid Foam; Strain Energy Release Rate

Introduction

Technical development facilitates an extensive use of foam core sandwich structures for load-bearing components in modern engineering (shipbuilding, car industry, aeronautics), where high strength and stiffness per weight are of primary importance (Gibson and Ashby, 1988; Reyes and Rangaraj, 2011; Christensen, 2000; Quispitupa et al., 2009; Shi-Dong Pan et al. 2008; Rangaraj, 2010). A sandwich structure typically consists of two thin stiff face sheets bonded to a relatively thick lightweight core. The face sheets mainly carry bending moments and axial loads as compressive or tensile stresses, while the core works in shear supports the faces against bucking and wrinkling. Sandwich structures provide additional advantages like very well acoustic and thermal insulation, high corrosion resistance, competetive energy absorption and buoyancy. The ability of a foam core sandwich structure to sustain loads essentially depends upon the properties of the foam core.

Crack initiation and propagation in the core significantly reduces the stiffness and may lead to failure of the sandwich structure. Therefore, it is of great practical importance to develop experimental and theoretical methods for investigation of the rigid foam fracture behavior.

Static fracture behavior of cellular foams has been previously investigated by Ashby et al. (1984). Static fracture in closed-cell foam under mode I loading conditions has also been studied by Bažant et al. (2003). Mode III static fracture toughness of rigid foam materials has been characterized by Farshad and Flüeler (1998) using an anti-clastic plate bending test method. A special loading device has been applied for inducing almost a pure mode III crack loading conditions in the foam specimen. An experimental and numerical investigation of debonding in foam core sandwich structures under static loading has been carried-out by Prassad and Carlsson (1994). Fracture tests have been performed using double cantilever beam and shear sandwich specimens. Test data have been analyzed by linear-elastic fracture mechanics concepts. For this purpose, two-dimensional finite element models have been developed. The models

have been verified by comparisons between the calculations and the measurements. Goswami and Becker (2001) have analyzed a static delamination crack along the face sheet/core interface in a sandwich structure subjected to transverse loading by a finite element model. The effect of different structural parameters on the face sheet/core delamination fracture has been studied. The Paris'law equation has been applied to characterize fatigue crack growth in foam material by Noble and Lilley (1981). The environmental effects on the fatigue fracture behavior of Polycarbonate foam material have been analyzed by Yau and Mayer (1986).

The present article describes an investigation of low-velocity impact fracture behavior of rigid foam using SENB specimens with inclined notch (it should be mentioned that such investigation has not been found in the literature available). In the experimental part of the study, low-velocity impact fracture tests were performed on SENB specimens with different notch inclinations. The basic purpose of the testing was to determine the critical impact potential energy and the fracture time at the onset of crack growth for different mixed-mode I/II crack loading conditions. Three-dimensional linear-elastic finite element simulations of the SENB specimens were carried-out in order to calculate the critical dynamic strain energy release rate using the experimental data.

Experimental Procedure

The foam under investigation in the present article is Divinycell HCP100. This is polyvinylchloride closed-cell foam with nominal density of 400 kg/m^3.

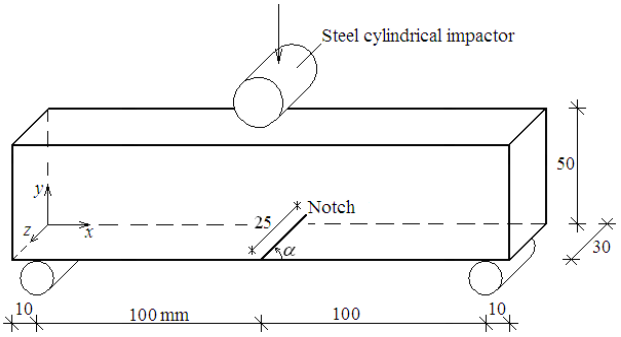

FIG. 1 GEOMETRY AND LOADING OF THE SENB SPECIMEN (THE ANGLE OF INCLINATION IS MARKED BY α)

Single edge notched bend specimens were cut-out by a diamond blade saw from foam panels according to FIG. 1. The length and the height of the specimen were L=220 mm and H=50 mm, respectively. The specimen width, W, was equal to the foam panel thickness (30 mm). An inclined notch with length of 25 mm was introduced as initial crack in the specimen mid-span. The notch inclination was varied from 15^0 to 90^0 with a step of 15^0 for the different specimens. The notch tip was sharpened by pressing a new razor blade in it prior to testing. None of the specimens was pre-cracked.

The SENB specimens were supported on two 12 mm diameter steel cylinders. The support span length was 200 mm (FIG. 1). The impact fracture tests were performed using a drop-weight rig. During testing the specimens were impacted at the mid-span by a steel cylinder with a diameter of 18 mm and length of 40 mm. After the first impact, the steel cylinder was captured to avoid secondary impacts. The impacting mass, 4.13 kg, was kept constant for all the tests. A range of impact potential energies were attained by varying the drop-height at each notch plane inclination in order to determine the critical energy. The tests were carried-out at room temperature (23^0C). Five replicate specimens were tested for each notch plane inclination. High repeatability of the test data was obtained. A computer system was used for data acquisition during testing. The contact force-time response was monitored continuously at each test.

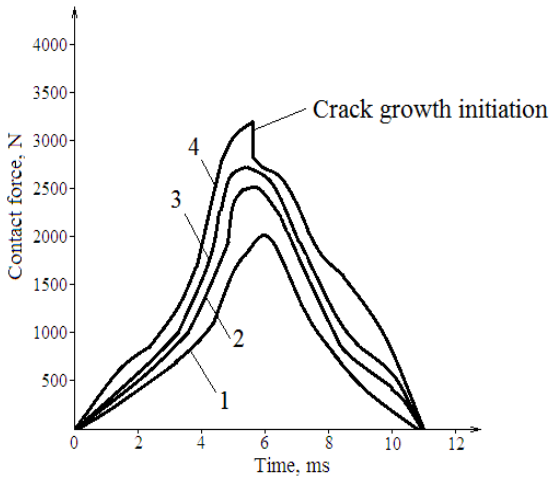

FIG. 2 EXPERIMENTALLY OBTAINED CONTACT FORCE-TIME RESPONSES OF THE SENB SPECIMEN WITH NOTCH INCLINATION OF 15^0 AT IMPACT POTENTIAL ENERGY OF 9.6 J (CURVE *1*), 13 J (CURVE *2*), 14 J (CURVE *3*), AND 14.8 J (CURVE *4*). THE CRACK GROWTH ONSET IN CURVE *4* IS SIGNALLED BY A SUDDEN DROP. THE TIME OF CRACK GROWTH INITIATION (I.E., THE FRACTURE TIME) IS t_f =5.5 ms

The onset of crack growth from the notch tip was determined by inspection of the specimen lateral surface with a microscope after each test (the notch tip position was marked on the specimen surface prior to testing). In this way it was found that the crack growth

in SENB specimen with notch inclination of 15^0 was initiated at impact potential energy level of 14.8 J. It should be noted that SENB specimens with notch inclination of 15^0 were tested at different impact potential energies. No crack growth was observed at energy levels lower than 14.8 J. Contact force-time curves for the various impact potential energies used in SENB specimen with notch inclination of 15^0 are depicted in FIG. 2. The data in FIG. 2 indicate that the maximum contact force generated during an impact fracture test increases with the impact potential energy, while the duration of the impact event (i.e. the time for which the impactor and the specimen are in contact) is almost constant for different impact potential energies. It was found that the crack growth initiation was signaled by a sudden drop in the contact force-time curve for the critical impact potential energy, E_{PC}, (FIG.2). This finding was attributed to the degradation of the SENB specimen bending stiffness due to the crack growth initiation. The time at the drop was recorded as the fracture time, t_f. It can be summarized that the experimental investigation yielded two important parameters (critical impact potential energy, E_{PC}=14.8 J, and fracture time, t_f=5.5 ms) which were used in the finite element analysis of the SENB specimen with notch inclination of 15^0 in order to evaluate the impact fracture toughness.

TABLE 1 MEASURED CRITICAL IMPACT POTENTIAL ENERGY, EPC, AND FRACTURE TIME, tC, AND CALCULATED AVERAGE TOTAL DYNAMIC CRITICAL STRAIN ENERGY RELEASE RATE, G_C^{Da}, MIXED-MODE RATIOS, G_{IC}^{Da}/G_C^{Da}, G_{IIC}^{Da}/G_C^{Da}, AND, G_{IIIC}^{Da}/G_C^{Da}, AND AVERAGE TOTAL STATIC CRITICAL STRAIN ENERGY RELEASE RATE, G_C^{Sa}, IN SENB SPECIMENS WITH DIFFERENT NOTCH PLANE INCLINATION, α.

α,^{0}	15	30	45	60	75	90
E_{PC}, J	14.8	13.4	12.2	11.5	10.8	10.4
t_C, ms	5.5	5.6	5.8	6.1	6.6	6.9
G_C^{Da}, J/m^2	3970	2853	2343	1907	1823	176
G_{IC}^{Da}/G_C^{Da}	0.51	0.53	0.59	0.64	0.81	1.00
G_{IIC}^{Da}/G_C^{Da}	0.43	0.41	0.35	0.33	0.17	0.00
G_{IIIC}^{Da}/G_C^{Da}	0.05	0.04	0.04	0.02	0.00	0.00
G_C^{Sa}, J/m^2	5117	3908	3301	2801	2492	224

The experimentally measured values of critical impact potential energy level and fracture time at notch inclination varying from 15^0 to 90^0 with a step of 15^0 are summarized in TABLE 1. One can see that the critical impact potential energy decreases with increasing the notch inclination. This finding was attributed to decrease of mode II component of crack loading and to decrease of SENB specimen bending stiffness with increase of the notch inclination.

Test Data Analysis

The impact fracture toughness was obtained from the test data using methods of linear-elastic fracture-mechanics. For this purpose, three-dimensional linear-elastic finite element models of the SENB specimens with different notch inclination under impact loading were developed using the ABAQUS/Explict program system.

FIG. 3 FINITE ELEMENT MESH USED IN THE SIMULATIONS OF THE SENB SPECIMEN WITH INCLINED NOTCH

The geometry and dimensions of the models were dictated by the SENB specimen configurations used in the low-velocity impact fracture tests. Due to the fact that the specimen had a plane of symmetry, and the width of the finite element model was reduced to 15 mm (i.e., only half of the SENB test specimen was considered in the modelling). This was done in order to reduce the finite elements number in the model and to decrease the computational time. Symmetric displacement boundary conditions *w=0* were applied at the plane of symmetry *z=15* mm [*w* is the nodal displacement components along the z-axis (the coordinate axes are shown in FIG. 1)]. The models were meshed using the 3-D continuous brick finite element C3D8R. This element is defined by 8 nodes (one at each corner) having three degrees of freedom per node (translations in the nodal *x*, *y*, and *z* directions). The mesh was condensed towards the crack front in order to perform a more accurate strain energy release rate analysis. A total of 29 250 elements were used in the modeling. Before carrying-out further calculations, a mesh sensitivity study was conducted with respect to the elements number in order to ensure that the mesh was fine enough to give reliable results. Typical mesh used in the simulations of the SENB

specimen is depicted in FIG. 3. The foam was modeled as a linear-elastic material in the finite element simulations with modulus of elasticity, E=340 MPa, and Poisson's ratio, ν=0.300. These elastic properties were experimentally measured according to the ASTM D 1621-94 methods. The steel impactor was modeled as a rigid body because its stiffness is much greater than that of the impacted SENB specimen. For this purpose, the rigid body modeling option was used. All rigid body motions of the impactor were removed except the translation in vertical direction. The contact-impact algorithm of the ABAQUS/Explict software was used to model the interface between the impactor and the specimen. In the finite element simulations the impactor was initially positioned just above the SENB specimen, subjected to gravitational force, and given an initial velocity which was estimated for the considered drop-height assuming ideal free fall with zero initial velocity.

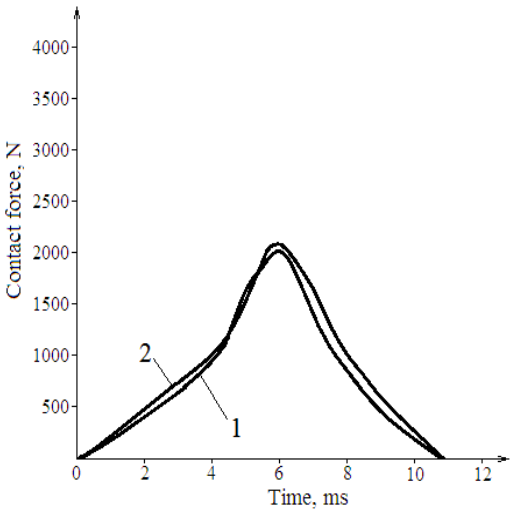

FIG. 4 CONTACT FORCE-TIME BEHAVIOUR OF THE SENB SPECIMEN WITH NOTCH INCLINATION OF 15⁰ AT IMPACT POTENTIAL ENERGY LEVEL OF 9.6 J. COMPARISON BEYWEEN THE EXPERIMENTAL DATA (CURVE *1*) AND THE FINITE ELEMENT COMPUTATIONS (CURVE *2*)

In order to verify the model, the calculated contact force-time curve was compared with the measured one, as shown in FIG. 4. It can be observed that the simulated and the experimental curves are in good agreement. Such comparisons were performed for various impact potential energy levels at each notch inclination used in the experimental testing. Good agreement between the computations and the measurements allowed us to validate the finite element models used to analyze the mechanical behavior of the SENB specimens under low-velocity impact loading.

In the present paper the impact fracture toughness was characterized in terms of the dynamic critical strain energy release rate, G_C^D, at the crack growth initiation from the notch tip.

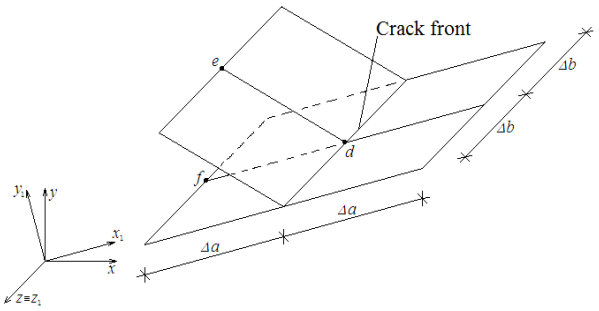

FIG. 5 SCHEMATIC OF THE CRACK FRONT ZONE WITH NODAL NOTATIONS

The dynamic critical strain energy release rate was computed using the virtual crack closure technique. The advantage of this technique is the fact that it requires only one analysis by the finite element model for the actual crack length. The nodal notations in the crack front zone are shown in FIG. 5. The virtual crack closure technique assumes that the work done to closure the crack by one length is equal to strain energy released when the crack grows by one element length. Therefore, the strain energy release rate mode components, G_I, G_{II}, and G_{III}, at node d in FIG. 5 can be calculated using the formulae

$$G_I = \frac{1}{2\Delta a \Delta b} X_{1d}\left(u_{1e} - u_{1f}\right), \quad (1)$$

$$G_{II} = \frac{1}{2\Delta a \Delta b} Y_{1d}\left(v_{1e} - v_{1f}\right), \quad (2)$$

$$G_{III} = \frac{1}{2\Delta a \Delta b} Z_{1d}\left(w_{1e} - w_{1f}\right), \quad (3)$$

where X1, Y1 and Z1 are the nodal force components, and u1, v1, and w1 are nodal displacements in the x1, y1 and z1 directions, respectively. The subscripts in Eqs. (1) – (3) denote the corresponding nodes in FIG. 5.

It has to be pointed out that the nodal force components X1 and Y1 in the local coordinate system x1y1z1, associated with the notch plane (FIG. 5) were

computed using the formulae for rotation of rectangular coordinates

$$X_1 = X\cos\alpha + Y\sin\alpha, \quad (4)$$

$$Y_1 = -X\sin\alpha + Y\cos\alpha, \quad (5)$$

where X and Y are the nodal force components in the global coordinate system, α is the angle of notch inclination which is defined in FIG. 1. The local coordinate system x1y1z1 is chosen in such way that coordinate plane x1z1 coincides with the notch plane [the z1-axsis is parallel to the crack front, the y1-axis is normal to the notch plane (FIG. 4)]. Thus, Z1- and Z - nodal force components coincide. The nodal displacement components u1 and v1 were computed from u and v using the same formulae for rotation of rectangular coordinates (w1 and w nodal displacement components coincide).

The components distribution of the strain energy release rate mode was obtained applying Eqs. (1) – (3) at each node along the crack front. The average values of the components of the strain energy release rate mode along the crack front were calculated as

$$G_I^a = \frac{1}{W}\int_0^W G_I(z)dz, \quad (6)$$

$$G_{II}^a = \frac{1}{W}\int_0^W G_{II}(z)dz, \quad (7)$$

$$G_{III}^a = \frac{1}{W}\int_0^W G_{III}(z)dz, \quad (8)$$

where $G_I(z)$, $G_{II}(z)$, and $G_{III}(z)$ are the components of the strain energy release rate mode along the crack front obtained by Eqs. (1) – (3).

The average value of the total strain energy release rate along the crack front was calculated as

$$G^a = G_I^a + G_{II}^a + G_{III}^a. \quad (9)$$

The distribution of dynamic strain energy release rate mode components, G_I^D, G_{II}^D, and G_{III}^D, along the crack front in the SENB specimen with stationary crack was obtained by Eqs. (1) - (3) at each step of the transient analysis for the experimentally determined critical impact potential energy for the notch inclination considered. The average values of the dynamic components in strain energy release rate mode, G_I^{Da}, G_{II}^{Da}, and G_{III}^{Da}, as well as the average value of the total dynamic strain energy release rate along the crack front, G^{Da}, were calculated by Eqs. (4) – (7) at each step of the transient analysis (the integrals in Eqs. (6) – (8) were solved numerically). In this manner G^{Da} was obtained in a function of the time as shown in FIG. 6 for notch inclination of 150 at the critical impact potential energy of 16 J.

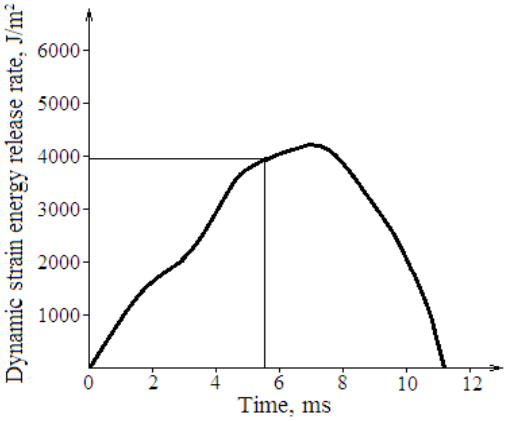

FIG. 6 AVERAGE VALUE OF THE DYNAMIC TOTAL STRAIN ENERGY RELEASE RATE ALONG THE CRACK FRONT, G^{Da}, PLOTTED AGAINST THE TIME AT THE CRITICAL IMPACT POTENTIAL ENERGY OF 14.8 J IN SENB SPECIMEN WITH NOTCH INCLINATION OF 15^0. THE IMPACT FRACTURE TOUGHNESS, $G_C^{Da} = 3970$ J/m², IS OBTAINED AT THE EXPERIMENTALLY MEASURED FRACTURE TIME, t_f =5.5 ms

The impact fracture toughness (expressed in terms of the average value of the total dynamic critical strain energy release rate along the crack front at the onset of crack growth from the notch tip), G_C^{Da}, was obtained at the experimentally determined fracture time, tf=5.5 ms, as illustrated in FIG. 6. In this way it was found $G_C^{Da} = 3970$ J/m2. The distribution of the dynamic critical strain energy release rate mode components, G_{IC}^D, G_{IIC}^D, and G_{IIIC}^D, along the crack front at tf=5.5 ms is shown in FIG. 7. Only half of the crack front is depicted, because the distribution is symmetrical about the crack front centre. The horizontal axis is defined such that z/W=0 is at the specimen lateral surface. Thus, z/W=0.5 corresponds to the crack front centre. It can be observed in FIG. 7 that the distribution is non-uniform with strong specimen lateral surface effects. Near the specimen lateral surface, there is a decrease in G_{IC}^D, an increase in G_{IIC}^D,

and appearance of G_{IIIC}^{D}. The mode III component arises as a result of different transverse contractions which occur in the crack faces.

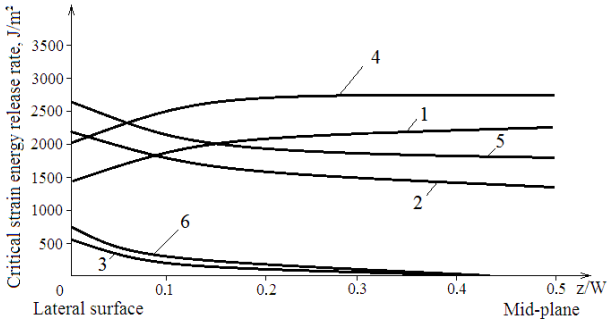

FIG. 7 DISTRIBUTION OF MODE I (CURVE *1*), MODE II (CURVE *2*), AND MODE III (CURVE *3*) COMPONENTS OF THE DYNAMIC CRITICAL STRAIN ENERGY RELEASE RATE AND MODE I (CURVE *4*), MODE II (CURVE *5*), AND MODE III (CURVE *6*) COMPONENTS OF THE STATIC CRITICAL STRAIN ENERGY RELEASE RATE ALONG THE CRACK FRONT IN SENB SPECIMEN WITH NOTCH INCLINATION OF 15^0. THE HORIZONTAL AXIS IS DEFINED SUCH THAT z/W=0 IS AT THE SPECIMEN LATERAL SURFACE; THUS z/W=0.5 CORRESPONDS TO THE CRACK FRONT CENTRE (W IS THE SPECIMEN WIDTH)

Such analyses of the components of the strain energy release rate mode were carried-out for each notch inclination from 150 to 900. Since the components of the strain energy release rate mode along the crack front was non-uniform, it was decided to characterize the fracture behavior by the average values of these components which were calculated using Eqs. (6) - (8). The corresponding integrals were solved numerically. The values of G_C^{Da} and the mixed-mode ratios, G_{IC}^{Da}/G_C^{Da}, G_{IIC}^{Da}/G_C^{Da}, and G_{IIIC}^{Da}/G_C^{Da}, obtained were summarized in TABLE 1. The data in TABLE 1 indicate that the average value of the total dynamic critical strain energy release rate, G_C^{Da}, decreases with increasing the notch plane inclination. This is due to the transition of the loading conditions in the notch tip from mixed-mode I/II at low notch plane inclination toward pure mode I at notch plane inclination of 900. In other words, when the notch is vertical, the analysis generates the pure mode I fracture toughness, while at notch tip inclinations less than 900, it generates mixed-mode I/II fracture toughness values which are higher than the mode I. It is interesting to analyze the evolution of the relative amount of mode II component of the dynamic critical strain energy release rate with increase of notch plane inclination. It can be seen in TABLE 1 that the ratio G_{IIC}^{Da}/G_C^{Da} decreases with increasing the inclination from 0.434 (at inclination of 150) to 0 (at inclination of 900). It can be summarized that the fracture performance is mode I dominated, because at each notch plane inclination the ratio G_{IC}^{Da}/G_C^{Da} is higher than 0.5. TABLE 1 indicates also that the relative amount of mode III component is very small compared with the mode II and the mode III. Therefore, the crack growth in SENB specimens containing inclined notch can be regarded as a mixed-mode I/II fracture problem.

The impact fracture toughness was compared with the static one at various notch inclinations. The static fracture toughness was experimentally characterized by the SENB specimens with inclined notch. The geometry and dimensions of the SENB specimens used in the static testing were the same as ones in the low-velocity impact fracture test. The specimens were loaded under displacement control at a constant cross-head speed of 3 mm/min. The test was stopped after about 4 mm crack extension. The critical fracture load at the onset of crack growth from the notch tip was determined by inspection of the specimen lateral surface using a microscope during the testing and by observation of the load-displacement response. The test data were analyzed by three-dimensional linear-elastic finite element models of the SENB specimens. The static critical components in the strain energy release rate mode (at the onset of static crack growth from the notch tip) were calculated by the virtual crack closure technique via Eqs. (1) – (3) applied at each node along the crack front. At notch inclination of 15o the calculations yielded the components of the strain energy release rate mode along the crack front that is shown in FIG. 7 for comparison with the dynamic critical strain energy release rate. The data in FIG. 7 indicate that the dynamic critical strain energy release rate is lower than the static one. The static fracture toughness, G_C^{Sa}, was calculated as the sum of the average values of the components of the strain energy release rate mode along the crack front using formula (9). Such analyses were carried-out for each notch inclination from 150 to 900. The obtained results are included in TABLE 1. It can be observed in Table 1 that the impact fracture toughness is between 22.4 % (at notch inclination of 150) and 32 % (at notch inclination of 600) lower than the static one. This finding is attributed to the brittle response of the polymer foam to the impact loading.

Conclusions

The impact fracture in rigid foam was investigated by SENB specimens with inclined notch. A drop-weight rig was used to perform the low-velocity impact fracture tests. The impact fracture behavior at various notch inclinations was studied in terms of the dynamic critical strain energy release rate at the onset of crack growth from the notch tip. From the experimentally obtained critical impact potential energy and the fracture time at various notch inclinations, the components of the strain energy release rate mode were determined by the virtual crack closure technique in conjunction with three-dimensional linear-elastic finite element dynamic analysis of the SENB specimen using the ABAQUS/Explicit software. Based on the obtained results, the following conclusions were drawn.

1. The onset of crack growth from the notch tip during the impact testing was signaled by a sudden drop in the contact force-time response of the SENB specimen. This finding is attributed to the specimen bending stiffness degradation due to the onset of crack growth.
2. The critical impact potential energy (at the onset of crack growth) decreases with increase of the notch inclination. This is due to the specimen bending stiffness decrease with increase of the notch inclination.
3. The developed finite element model can be used for analyzing the mechanical response of the SENB specimen to impact loading, since the computed contact force-time curves were in a very good agreement with the measured ones at various impact potential energy levels and notch inclinations.
4. Non-uniform distribution of the dynamic critical strain energy release rate mode components along the crack front with strong specimen lateral surface effects was generated by the analysis.
5. It was found that the SENB specimen with notch inclination varying from 150 to 900 can be used for experimental investigation of impact mixed-mode I/II fracture behavior of rigid foams over the range of $0 \le G_{IIC}^{Da} / G_{C}^{Da} \le 0.434$.
6. The impact fracture toughness was between 22.4 % (at notch inclination of 150) and 32 % (at notch inclination of 600) lower than the static one (this finding is attributed to the brittle response of the polymer foam to the impact loading). Thus, the static fracture toughness should not be used in the fracture mechanics based design of rigid foam structures that are subjected to impact loading during their lifetime.

REFERENCES

Ashby, M.F., L.J. Gibson, and S.K. Maiti. „Fracture Toughness of Brittle Cellular Solids." Scr. Metall. 18 (1984): 213 - 217.

Bažant, Z.P., Y. Zhou, G. Zi, and I. Daniel. „Size effect and asymptotic matching analysis of fracture of closed-cell polymeric foam." International Journal of Solids and Structures 40 (2003): 7197 - 7217.

Christensen, R.M. „Mechanics of cellular and other low-density materials. " Int. J. Sol. Struct. 3 (2000): 93-104.

Farshad, M., and P. Flüeler. „Investigation of mode III fracture toughness using an anti-clastic plate bending method." Engineering Fracture Mechanics 60 (1998): 597 - 603.

Gibson, L. J., and M. F. Ashby. Cellular solids – structure and properties. Oxford: Paramount Press, 1988.

Goswami, S., and W. Becker. „The effect of face sheet/core delamination in sandwich structures under transverse loading. " Composite structures 54 (2001): 515 – 521.

Noble, F. W., and J. Lilley. „Fatigue Crack Growth in Polyurethane Foam." Journal of Materials Science 16 (1981): 800 – 1808.

Prassad, S., and L.A. Carlson. „Debonding and crack kinking in foam core sandwich beams – I. Analysis of fracture specimens." Engng. Fracture Mech. 47 (1994): 813 – 824.

Prassad, S., and L.A. Carlson. „Debonding and crack kinking in foam core sandwich beams – II. Experimental investigation." Engng. Fracture Mech. 47 (1994): 825 – 841.

Quispitupa, A., C. Berggreen, and L.A. Carlsson. „On the analysis of a mixed mode bending sandwich specimen for fracture characterization." Engineering Fracture Mechanics 76 (2009): 594-613.

Rangaraj, S. „Influence of skin/core debonding on free vibration behaviour of foam and honeycomb cored sandwich plates." Journal of Non-Linear Mechanics 45v(2010): 959-968.

Reyes, G., and S. Rangaraj. "Fracture properties of high performance carbon foam sandwich structures." Composites Part A: Applied Science and Manufacturing 42 (2011): 1-7.

Shi-Dong Pan, Lin-Zhi Wu, Yu-Guo Sun, and Zheng-Gong Zhou. "Fracture test for double cantilever beam of honeycomb sandwich panels." Materials Letters 62 (2008): 523-526.

Yau, S.S., and G. Mayer. "Fatigue Crack Propagation in Polycarbonate Foam." Journal of Materials Science and Engineering 78 (1986): 111 – 114.